Discovery of anti-inflammatory physiological peptides that promote tissue repair by reinforcing epithelial barrier formation

AUTHOR(S):

Oda, Yukako; Takahashi, Chisato; Harada, Shota; Nakamura, Shun; Sun, Daxiao; Kiso, Kazumi; Urata, Yuko; ... Uchida, Seiichi; Ishihama, Yasushi; Toyoshima, Fumiko

CITATION:

Oda, Yukako ...[et al]. Discovery of anti-inflammatory physiological peptides that promote tissue repair by reinforcing epithelial barrier formation. Science Advances 2021, 7(47): eabj6895.

ISSUE DATE:

2021-11-19

URL:

http://hdl.handle.net/2433/266092

CELL BIOLOGY

Discovery of anti-inflammatory physiological peptides that promote tissue repair by reinforcing epithelial barrier formation

Yukako Oda[1]*, Chisato Takahashi[2,3], Shota Harada[4], Shun Nakamura[5,6], Daxiao Sun[7], Kazumi Kiso[1], Yuko Urata[1], Hitoshi Miyachi[8], Yoshinori Fujiyoshi[5,6], Alf Honigmann[7], Seiichi Uchida[4], Yasushi Ishihama[2], Fumiko Toyoshima[1]

Epithelial barriers that prevent dehydration and pathogen invasion are established by tight junctions (TJs), and their disruption leads to various inflammatory diseases and tissue destruction. However, a therapeutic strategy to overcome TJ disruption in diseases has not been established because of the lack of clinically applicable TJ-inducing molecules. Here, we found TJ-inducing peptides (JIPs) in mice and humans that corresponded to 35 to 42 residue peptides of the C terminus of alpha 1-antitrypsin (A1AT), an acute-phase anti-inflammatory protein. JIPs were inserted into the plasma membrane of epithelial cells, which promoted TJ formation by directly activating the heterotrimeric G protein G13. In a mouse intestinal epithelial injury model established by dextran sodium sulfate, mouse or human JIP administration restored TJ integrity and strongly prevented colitis. Our study has revealed TJ-inducing anti-inflammatory physiological peptides that play a critical role in tissue repair and proposes a previously unidentified therapeutic strategy for TJ-disrupted diseases.

INTRODUCTION

Epithelial cells have barrier functions that separate internal compartments of the body from the outside environment to maintain homeostasis of multicellular organisms. In vertebrates, this barrier function requires tight junctions (TJs) that bond adjacent cells in epithelial tissues throughout life. TJs consist of multiple protein complexes including the transmembrane proteins claudins and cytosolic adapter zonula occludens (ZO) (*1*–*7*). Knockout or knockdown of claudin family genes in mice impairs the functional barrier, which leads to neonatal lethality or various diseases, including electrolyte abnormalities and inflammatory diseases such as dermatitis, hepatitis, and colitis (*8*, *9*).

In response to tissue injury and inflammation, the epithelium is repaired by epithelial cell self-renewal and barrier reconstruction, which are mediated by the interplay of epithelial cells and infiltrating immune cells (*10*). Although the intestinal epithelium regenerates from Lgr5-negative epithelial cells during recovery in colonic injury models (*11*), the mechanism of TJ reconstitution during epithelial tissue repair remains unclear.

Here, we searched for tissue damage–responding TJ-inducing humoral factors from mouse epithelium and identified C-terminal fragments of alpha 1-antitrypsin (A1AT), which we designated as TJ-inducing peptides (JIPs). Similar peptides have been found in sera of humans with various inflammatory diseases (*12*–*14*). Our data demonstrate a critical role of JIPs in TJ reconstruction of the intestinal epithelium during recovery in a colonic injury model and reveal the underling mechanism of JIP-inducing TJ formation. We also demonstrate the clinical relevance of JIPs for acute tissue destruction.

RESULTS

A1AT C-terminal peptides are tissue damage–responding JIPs

To assess TJ reconstitution during epithelial tissue repair, we analyzed recovery from a dextran sulfate sodium (DSS)–induced colitis model in mice. Claudin-3 apico-lateral localization of intestinal epithelial cells in control mice was impaired in DSS-treated mice as reported for ZO-1 (*15*). However, TJs were reconstituted at 2 days after recovery from DSS treatment (Fig. 1, A and B). Unexpectedly, conditioned medium prepared from colon culture supernatant (CCM) had an activity that induced claudin assembly at cell-cell boundaries in human A431 epidermoid carcinoma cells that usually do not assemble TJ structures (Fig. 1, C and D) (*16*). CCM from recovery day 1 mice exhibited the highest claudin-assembling activity (Fig. 1E and fig. S1, A and B). Conditioned medium of peritoneum culture (PCM) also had a claudin-1–assembling activity that was increased by lipopolysaccharide (LPS) administration (fig. S1, C to E). Permeability analysis confirmed that PCM treatment promoted the barrier potential of A431 cell monolayers (fig. S1F). Notably, the protein level of claudin-1 was unchanged in A431 cells when treated with or without PCM (fig. S1G), indicating that PCM induced claudin assembly in a mechanism that is independent of claudin-1 gene expression regulation. Furthermore, PCM treatment induced or enhanced claudin assembly at cell-cell boundaries of MCF7, HT29, and EpH4 cells (fig. S2, A to F). These results showed that CCM and PCM contained a TJ-inducing humoral factor(s) that accumulated after inflammation.

[1]Department of Biosystems Science, Institute for Frontier Life and Medical Sciences, Kyoto University, Kyoto 606-8507, Japan. [2]Department of Molecular and Cellular BioAnalysis, Graduate School of Pharmaceutical Sciences, Kyoto University, Kyoto 606-8501, Japan. [3]Laboratory of Analytical Chemistry, Faculty of Pharmaceutical Sciences, Doshisha Women's College of Liberal Arts, Kyoto 610-0395, Japan. [4]Laboratory of Human Interface, Graduate School of Systems Life Sciences, Kyushu University, Fukuoka 819-0395, Japan. [5]Cellular and Structural Physiology Laboratory, Advanced Research Institute, Tokyo Medical and Dental University, Tokyo 113-8510, Japan. [6]CeSPIA Inc., Tokyo 100-0004, Japan. [7]Max Planck Institute of Molecular Cell Biology and Genetics, Dresden 01309, Germany. [8]Reproductive Engineering Team, Institute for Frontier Life and Medical Sciences, Kyoto University, Kyoto 606-8507, Japan.
*Corresponding author. Email: ykoda@infront.kyoto-u.ac.jp

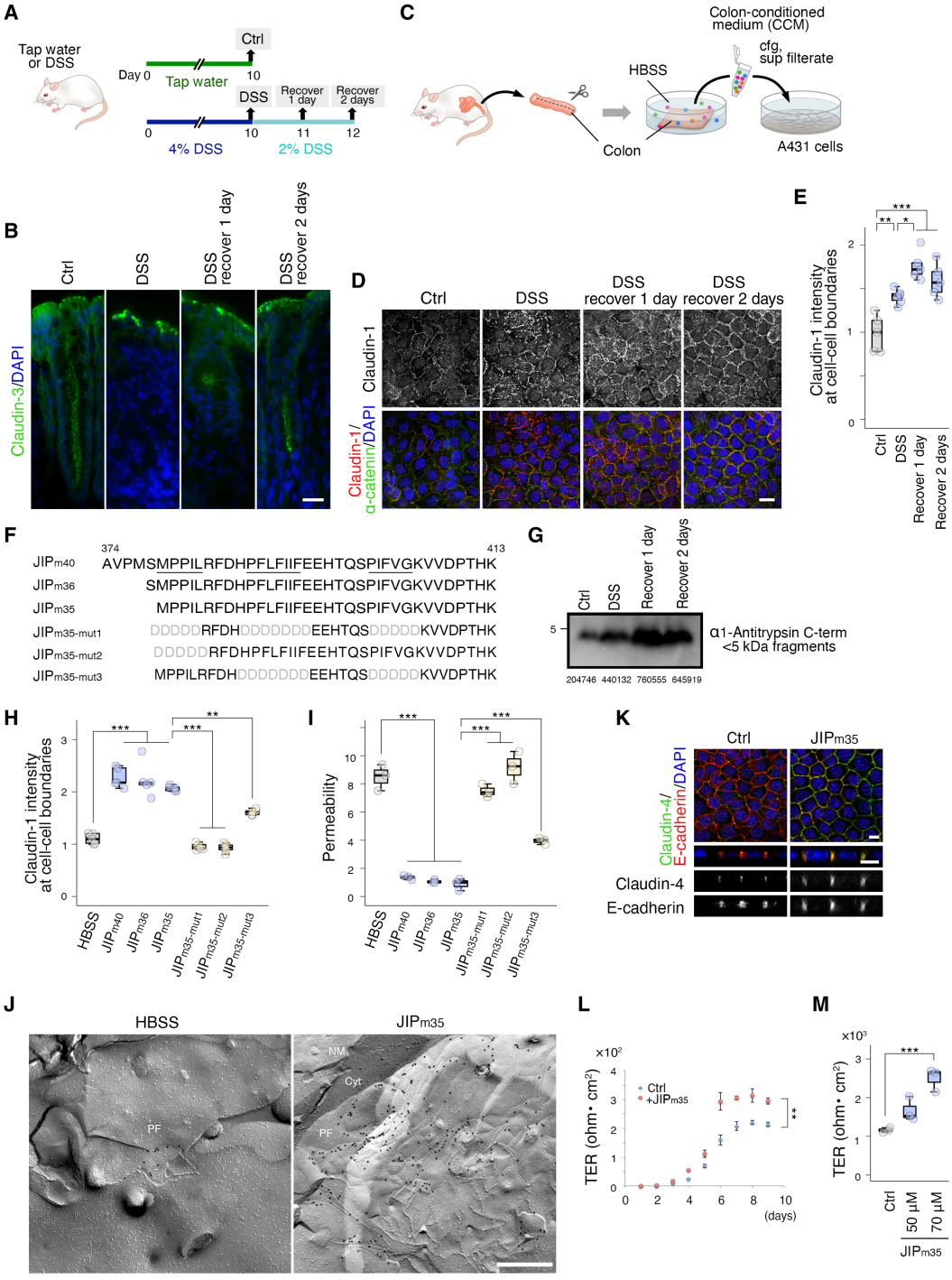

Fig. 1. A1AT C-terminal peptides induce TJ assembly. (**A**) Schema of recovery from the DSS-induced colitis model in mice. (**B**) Immunofluorescence of claudin-3 and DAPI in colon sections from mice treated as in (A). Scale bar, 20 μm. (**C**) Schema of the CCM treatment of A431 cells. (**D**) Immunofluorescence of claudin-1 and α-catenin in A431 cells treated for 3 hours with CCM from mice treated as in (A). Scale bar, 20 μm. (**E**) Quantification of relative claudin-1 intensity at cell-cell boundaries shown in (D) [$n = 5$ images (ctrl and recover), $n = 6$ images (DSS) from two independent samples]. (**F**) Amino acid sequences of the JIP_{m35}, JIP_{m36}, and JIP_{m40}. (**G**) Western blot of CCM with anti-A1AT C terminus antibodies. Quantitative value of each band was presented. (**H**) Quantification of relative claudin-1 intensity at cell-cell boundaries of A431 cells treated with the indicated peptides (20 μM) or HBSS for 3 hours. See fig. S5B ($n = 5$ images from two independent samples). (**I**) Relative barrier permeability of A431 cells ($n = 3$ independent samples). (**J**) Immuno freeze-fracture replica electron microscopy of A431 cells treated with JIP_{m35} (20 μM) or HBSS and immunolabeled with anti–claudin-1 antibodies. NM, nuclear membrane; Cyt, cytoplasm; PF, P face. Scale bar, 500 nm. (**K**) Immunofluorescence of claudin-4 and E-cadherin in EpH4 cells treated with or without JIP_{m35} (70 μM) for 3 hours. Scale bars, 10 μm. (**L**) TER measurements of EpH4 cells treated with or without JIP_{m35} for 3 hours (70 μM, $n = 3$ independent samples). (**M**) TER measurements of EpH4 cells treated with or without JIP_{m35} for 3 hours at day 6 ($n = 3$ independent samples). Tukey's test (E), (H), and (I), and two-tailed t test (L) and (M). $^*P < 0.05$, $^{**}P < 0.01$, $^{***}P < 0.001$. Similar results were obtained in two independent experiments in (B), (E), (G), (H), and (J).

The TJ-inducing molecule(s) in PCM was heat stable (fig. S3, A to C) with a molecular mass of 1.0 to 3.5 kDa (fig. S3D). We purified TJ-inducing molecules from heat-treated PCM by sequential chromatography on Q Sepharose and Con A Sepharose (fig. S4, A to D) and then identified them by trypsin digestion and nano-liquid chromatography (LC)/mass spectrometry (MS)/MS analysis. We identified 67 peptides that corresponded to 22 proteins, among which 3 were extracellular proteins, all of which belonged to the serpin A family of secretory proteins, including A1AT (fig. S4E, source data fig. 1). The C18 column chromatogram of anti-A1AT immunoprecipitates showed three peaks for claudin-assembling activity (fig. S4, F to J). MS analysis of the fractions identified four peptides [22, 35, 36, and 40 amino acids (aa)], all of which corresponded to the C-terminal region of A1AT (fig. S4K, source data figs. 2 to 5). Synthetic peptides of the 35, 36, and 40 aa, but not 22 aa, showed peaks in active fractions (fig. S4L, see H). We therefore designated the 35, 36, and 40 aa peptides as putative JIPs (Fig. 1F). Intriguingly, antibodies against JIPs (anti-JIPs Ab) (fig. S5A) indicated that JIPs had accumulated in CCM during DSS treatment and recovery and in PCM after LPS treatment (Fig. 1G and fig. S1H). Critically, synthetic JIP_{m35}, JIP_{m36}, and JIP_{m40} induced claudin assembly at cell-cell boundaries (Fig. 1H and fig. S5B) and promoted the barrier activity of A431 cell monolayers (Fig. 1I). Other TJ components, including ZO-1 and occludin, were also recruited to cell-cell boundaries by JIP_{m35} (fig. S5C). Freeze-fracture electron microscopy showed that JIP_{m35} induced a cluster of TJ strands, but not the mature form of a ribbon-like TJ structure (*17*) in A431 cells (Fig. 1J). Consistently, JIP_{m35} did not increase transepithelial resistance (TER) values of A431 cell monolayers (fig. S5, D and E), which indicated that JIP_{m35} induced an immature form of TJs in A431 cells. However, JIP_{m35} increased TER values in EpH4, MCF7, and HT29 cell monolayers (Fig. 1, K to M, and fig. S5, F to I), which suggested that the properties of JIP_{m35}-induced TJs varied between cell types. Notably, JIP_{m35} had no serine protease inhibitory activity against trypsin, elastase, or chymotrypsin (fig. S6, A to D), a well-known function of full-length (FL) A1AT (*18*). These data indicate that A1AT C-terminal peptides function as tissue damage–responding JIPs that promote TJ formation by a mechanism independent of protease inhibitory activity. Moreover, JIP_{m35} did not reduce LPS-induced release of proinflammatory cytokines [tumor necrosis factor–α (TNFα) and C-X-C motif chemokine ligand 1 (CXCL1)] from mouse neutrophils (fig. S6, E and F), which suggested that JIPs had no or little if any immunosuppressive effects on neutrophil activation.

JIPs are required for TJ restoration during tissue repair

To assess the role of JIPs in TJ restoration during tissue repair, we used the neutralizing activity of anti-JIPs Ab, which inhibited JIP_{m35}-induced claudin-1/ZO-1/occludin assembly at cell-cell boundaries of A431 cells (fig. S7, A to C) and suppressed JIP_{m35}-induced TER enhancement in EpH4 cell monolayers (fig. S7D). We administrated anti-JIPs Ab intraperitoneally into *Lgr5creERT2;R26-tdTomato* mice, which label intestinal epithelial cells (*19*), and analyzed reconstitution of intestinal crypt structures and epithelial TJs upon recovery from DSS treatment (Fig. 2A). We observed fully Tomato-labeled crypts in both preimmune and anti-JIPs Ab administration, suggesting that administration of anti-JIPs Ab at the onset of recovery had a minor effect on crypt regeneration. However, restoration of ZO-1 apico-lateral localization at recovery day 2 was impeded (Fig. 2B and fig. S11A), and restoration of the stool condition and suppression of Gr-1–positive neutrophil infiltration into epithelial layers at recovery day 2 was significantly reduced in anti-JIPs Ab–injected mice (Fig. 2, C and D). Furthermore, intestinal barrier integrity at recovery day 2 was significantly reduced in anti-JIPs Ab–injected mice (Fig. 2E). These results indicate that JIPs have a critical role in TJ reconstitution of intestinal epithelial cells during tissue repair.

Matrix metalloproteinases (MMPs) cleave human (h)A1AT in the C-terminal region (Fig. 5A) (*20*–*24*). To assess the functional relevance of MMPs to TJ formation, FL-hA1AT recombinant protein was treated with MMP-1, MMP-8, or MMP-9. MMP-treated FL-hA1AT generated ~5-kDa fragments of the 37–amino acid A1AT C-terminal peptides (Fig. 2F, source data figs. 6 to 8) and induced claudin assembly at cell-cell boundaries of A431 cells, whereas FL-hA1AT or MMPs alone did not show a TJ-inducing activity (Fig. 2G and fig. S7E). In addition, CCM prepared from colon tissues in the presence of MMP inhibitor GM6001 had an attenuated claudin-assembling activity at DSS recovery day 1 (Fig. 2H and fig. S7F). These data show that A1AT acquires TJ-inducing activity upon cleavage by MMPs.

JIPs penetrate the plasma membrane and activate G13 to induce TJ assembly

Next, we investigated the mechanism by which JIPs induce TJ assembly. Exogenously applied JIP_{m35} was localized at cell-cell boundaries of A431 cells (fig. S8A), which suggested that JIPs function on plasma membranes. Intriguingly, JIPs harbored three hydrophobic amino acid clusters (Fig. 1F). Claudin-assembling activity was significantly reduced when the N-terminal hydrophobic cluster or C-terminal hydrophobic clusters were replaced by a hydrophilic amino acid, Asp (Fig. 1, H and I, and fig. S5B; $JIP_{m35\text{-}mut1}$, $JIP_{m35\text{-}mut2}$, and $JIP_{m35\text{-}mut3}$), which indicated that the N-terminal and C-terminal hydrophobic amino acid clusters are essential for the TJ-assembling activity of JIPs. Because hydrophobic amino acid clusters can insert into the plasma membrane, we hypothesized that JIPs penetrate plasma membranes. To test this, we introduced anti-JIPs Ab into the cytosol, and cells were treated with or without JIP_{m35}. Intracellularly introduced anti-JIPs Ab, but not control preimmune serum, shifted from the cytosol to cell-cell boundaries upon JIP_{m35} treatment (Fig. 3A and fig. S8, B and C). This indicated that the antibody epitopes resided intracellularly and that JIP_{m35} penetrated the plasma membrane. In addition, a liposome pull-down assay showed that JIP_{m35} and $JIP_{m35\text{-}mut2}$, but not $JIP_{m35\text{-}mut1}$, were coprecipitated with liposomes, which indicated that JIP_{m35} associates with lipid bilayers through C-terminal hydrophobic clusters (Fig. 3B and fig. S8D). These results suggest that JIP_{m35} interacts directly with cytosolic proteins by penetrating the plasma membrane.

PCM treatment of claudin-deficient L cells and HeLa cells (*25*, *26*) resulted in patch-like assembly of ZO-1 proteins at cell-cell boundaries (fig. S8, E to H), which suggested that JIPs assemble ZO-1 in a claudin-independent manner. It has been reported that phase separation of ZO proteins drives TJ formation (*27*). However, JIP_{m35} had no significant effect on in vitro ZO-1 phase separation assays (fig. S8I) or recruitment of ZO-1 proteins to liposome membranes (fig. S8J). These results suggest that JIP_{m35} promotes TJ assembly via a pathway upstream of ZO proteins.

Trimeric G protein–coupled receptors induce TJs (*28*, *29*). Because JIP_{m35} was localized under the cell membrane, we examined

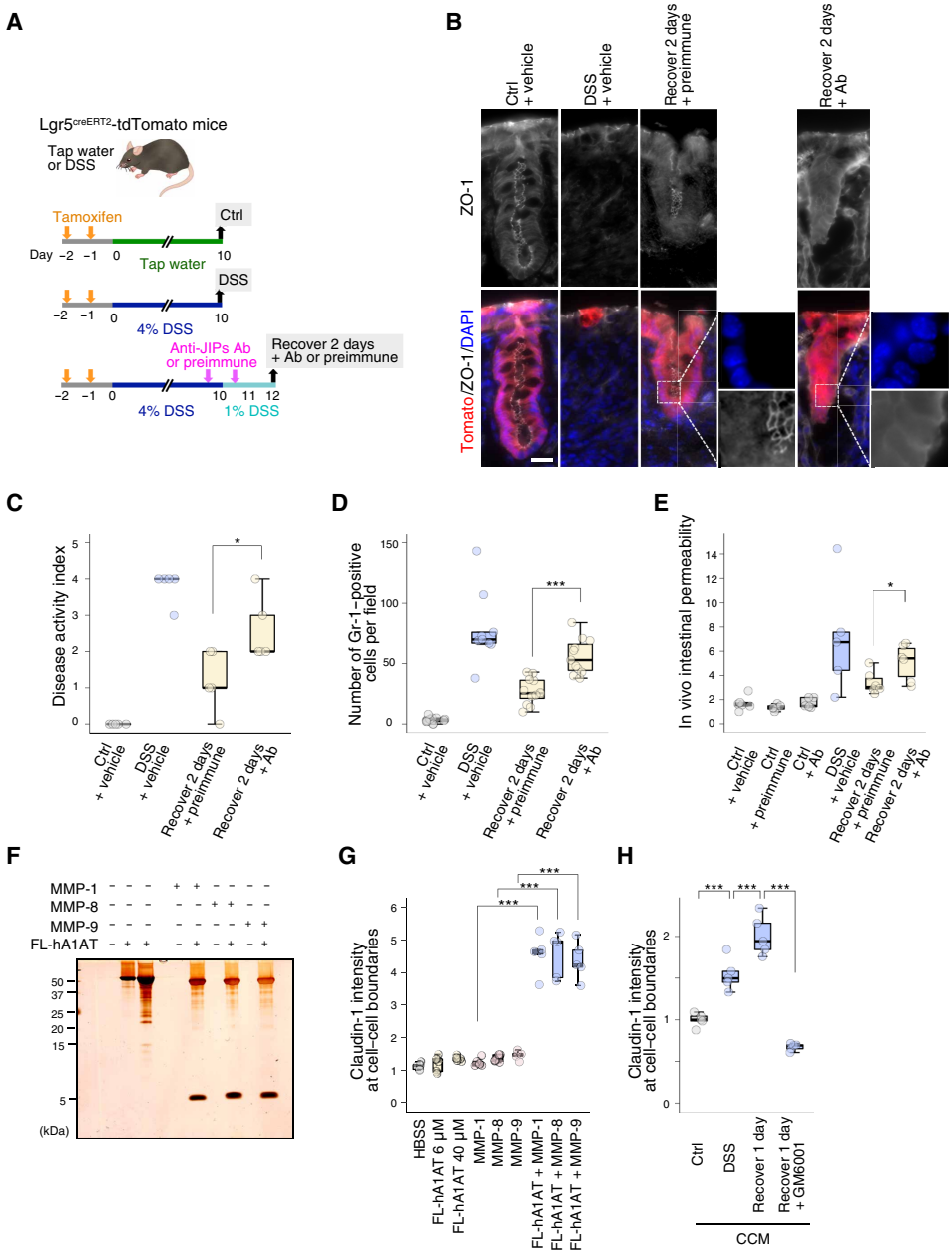

Fig. 2. JIPs are produced by MMP-mediated cleavage from A1AT and promote TJ reconstruction during recovery from the DSS-induced colitis model in mice. (**A**) Schema of anti-JIPs Ab administration to *Lgr5-EGFP-IRES-creERT2/tdTomato* mice with DSS-induced colitis at the recovery stage. (**B**) Immunofluorescence of ZO-1 and DAPI in colon sections from mice treated as in (A). Scale bar, 20 μm. Similar results were obtained in two independent experiments. (**C**) DAI in accordance with assessment of stool consistency and fecal blood in ICR mice, in which 2% DSS was used for recovery ($n = 5$ mice). (**D**) Quantification of the numbers of Gr-1–positive cells (9 to 12 images from five mice) treated as described in (C). (**E**) Relative intestinal permeability measured by plasma leakage of FITC-dextran (4 kDa) treated as described in (C) ($n = 5$ mice from ctrl + preimmune or Ab, DSS + vehicle, $n = 6$ mice from ctrl + vehicle, recover + preimmune or Ab). (**F**) Silver staining of recombinant hA1AT incubated with or without MMP-1, MMP-8, or MMP-9. Similar results were obtained in two independent experiments. (**G**) Quantification of relative claudin-1 intensity at cell-cell boundaries of A431 cells treated with the indicated products or control HBSS ($n = 5$ images from independent two samples). Similar results were obtained in two independent experiments. See fig. S7E. (**H**) Quantification of the relative claudin-1 intensity at cell-cell boundaries of A431 cells treated with CCM prepared from control, DSS-treated mice, or DSS-recovery mice in the presence or absence of GM6001, or control HBSS for 3 hours ($n = 5$ images from independent two samples). Similar results were obtained in two independent experiments. See fig. S7F. Tukey's test (C, D, G, and H) and the two-tailed *t* test (E). $^*P < 0.05$, $^{***}P < 0.001$.

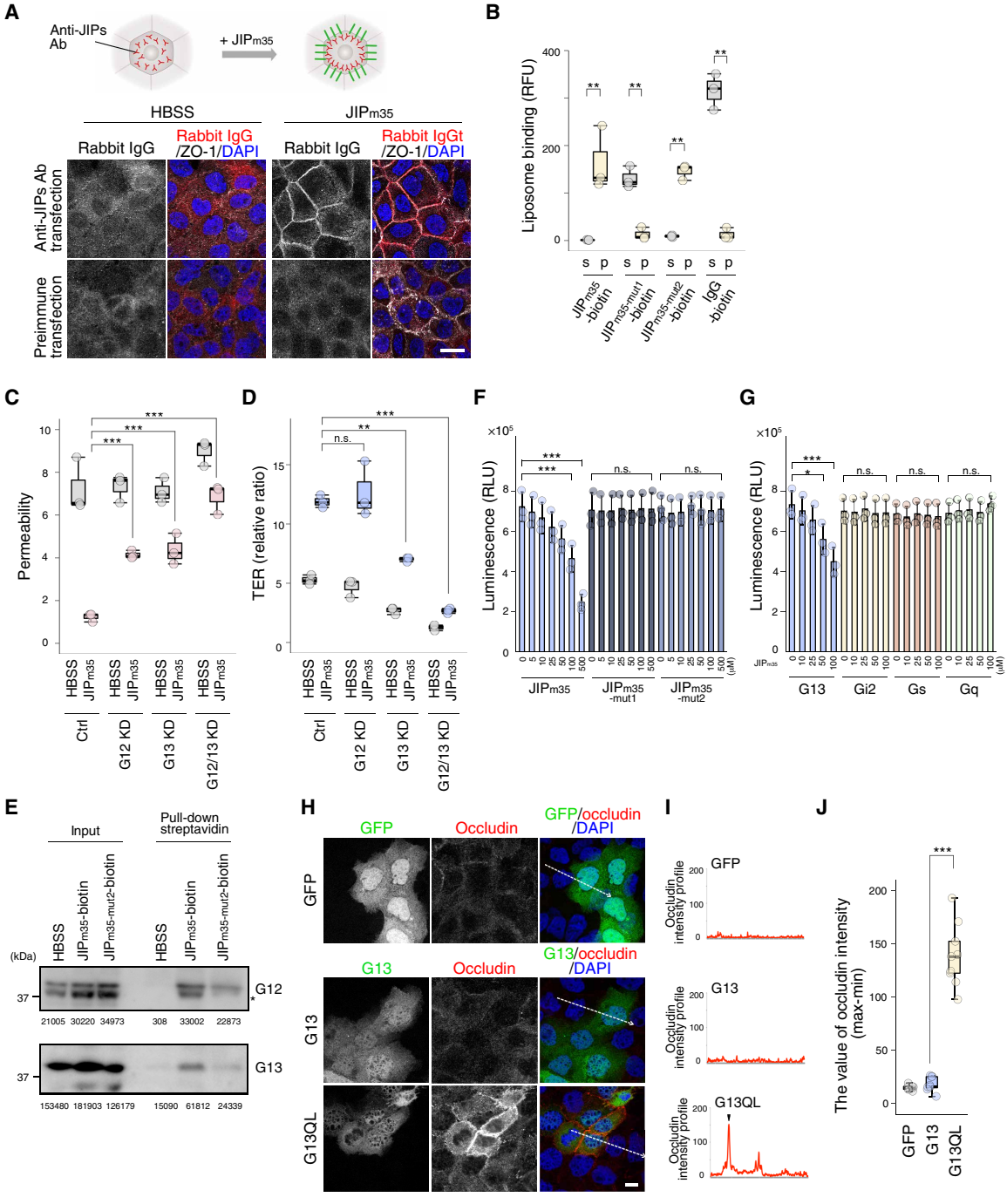

Fig. 3. JIPs penetrate the plasma membrane lipid bilayer and activate heterotrimeric G protein G_{13}. (**A**) Immunofluorescence of rabbit IgG and ZO-1 in A431 cells transfected with anti-JIPs Ab or preimmune. Transfected cells were treated with JIP_{m35} (20 μM) or HBSS for 3 hours. Scale bar, 20 μm. (**B**) Liposome cosedimentation assay using biotinylated JIP_{m35} peptides or IgG (20 nmol each), which were bound to streptavidin-FITC ($n = 3$ independent samples). (**C**) Relative barrier permeability measured by paracellular tracer flux analysis using FITC-dextran (4 kDa) in A431 cells transfected with G_{12} and/or G_{13} siRNA. See fig. S10B ($n = 3$ independent samples). (**D**) TER measurements of EpH4 cells transfected with G_{12} and/or G_{13} siRNAs. See fig. S10D ($n = 3$ independent samples). (**E**) Pull-down assay of A431 cells treated with biotinylated-JIP_{m35}, biotinylated-$JIP_{m35\text{-}mut2}$, or buffer using streptavidin-Sepharose. Precipitates were immunoblotted with anti-G_{12} (upper), G_{13} (bottom) antibodies. Asterisk indicates a nonspecific band. Quantitative value of each band was presented. (**F**) Measurement of G_{13} activation by JIP_{m35}, $JIP_{m35\text{-}mut1}$, and $JIP_{m35\text{-}mut2}$ ($n = 3$ independent samples). JIP_{m35} was prepared at the indicating concentrations. (**G**) Measurement of G protein (G_{13}, G_{i2}, G_s, and G_q) activation by JIP_{m35} ($n = 3$ independent samples). (**H**) Immunofluorescence of occludin, GFP, and G_{13} in A431 cells transfected with GFP, G_{13}, or G13Q226L. Scale bar, 10 μm. (**I**) Line scans represent the fluorescence intensity of occludin along the white arrow in (H), and a black arrowhead represents the position of cell junction. (**J**) The value represents the maximum value minus the minimum value of occludin intensity ($n = 9$ cells). Data represent means ± SD (F and G); Tukey's test (B and J) and Dunnett's test (C, D, F, and G). n.s., not significant. $^*P < 0.05$, $^{**}P < 0.01$, $^{***}P < 0.001$. Similar results were obtained in two independent experiments in (A) and (E).

the possibility of direct activation of G protein alpha subunits by JIPs. Treatment of A431 cells with *Pasteurella multocida* toxin, which activates G_i, G_q, and $G_{12/13}$ (*30*, *31*), but not with G_s-activating cholera toxin (*32*), induced TJ assembly (fig. S9, A to C). Inhibition of either G_s, G_i, or G_q by NF449 (*33*), pertussis toxin (*34*), or YM-254890 (*35*), respectively, did not reduce JIP_{m35}-mediated TJ assembly (fig. S9, D and E). Conversely, small interfering RNA (siRNA)–mediated knockdown of $G_{12/13}$ suppressed JIP_{m35}-induced claudin/ZO-1/actin assemblies at cell-cell boundaries of both A431 and EpH4 cells (fig. S10, A to D) and attenuated JIP_{m35}-induced barrier activity in monolayers of these cells (Fig. 3, C and D). Ectopic expression of a constitutively active form of G_{13} (G_{13}QL), but not wild-type G_{13}, induced occludin assembly at cell-cell boundaries of A431 cells (Fig. 3, H to J), which indicated that G_{13} activation is sufficient to assemble TJ components. These results indicate that JIP_{m35} induces TJ assembly via $G_{12/13}$.

JIP_{m35} pull-down assays showed that JIP_{m35} bound to endogenous $G_{12/13}$ proteins in A431 cells, and this interaction was reduced by $JIP_{m35\text{-}mut2}$ (Fig. 3E). In addition, G_{13} protein activity, which was measured by exchange of the guanine nucleotide in in vitro reactions, was increased by JIP_{m35} in a dose-dependent manner but not by $JIP_{m35\text{-}mut1}$ or $JIP_{m35\text{-}mut2}$ (Fig. 3F), which indicated that JIP_{m35} directly binds to and activates G_{13} through the N-terminal hydrophobic cluster. JIP_{m35} activated G_{13}, but not G_i, G_s, or G_q (Fig. 3G and fig. S10E), which demonstrated the specificity of JIP_{m35} for G13. Together, these results demonstrate that JIPs insert into plasma membranes and induce TJ assembly by directly activating G_{13}.

Administration of mouse or human JIPs restores TJs and ameliorates the symptoms of DSS-induced colitis in mice

We next examined whether JIPs restore TJs in the intestinal epithelium of a mouse colitis model. Administration of JIP_{m35} to DSS-treated mice every other day for 10 days sustained epithelial TJs and crypt structures, whereas $JIP_{m35\text{-}mut1}$ did not show these effects (Fig. 4, A to C and fig. S11B). In addition, the intestinal barrier integrity was sustained in DSS-treated mice by JIP_{m35} administration (Fig. 4D). Notably, immunofluorescence signals of the administered JIP_{m35} were detected at cell-cell boundaries of intestinal epithelial cells (Fig. 4E), which suggested that JIP_{m35} restored TJs by acting on epithelial cells in vivo. JIP_{m35} administration resulted in no marked changes in epithelial TJs or crypt structures in control mice (Fig. 4, B to D, and fig. S11B), which suggested that JIPs facilitate TJ reassembly only in damaged epithelial cells.

We next investigated whether JIPs alleviated the symptoms of DSS-treated mice. Hematogenous diarrhea (Fig. 4F and fig. S11C) and inflammation-associated infiltration of Gr-1–positive neutrophils within epithelial layers (Fig. 4G and fig. S11D) were ameliorated by administration of JIP_{m35} but not by $JIP_{m35\text{-}mut1}$ (Fig. 4, F and G, and fig. S11, C and D). In addition, consecutive administrations of JIPm35 starting at 4 days after DSS treatment, when the mice had manifested the bloody feces symptom, alleviated DSS-induced body loss and sustained survival for >4 weeks (Fig. 4, H and I). No significant changes in body weight or the survival rate were observed after administration of JIP_{m35} to control mice during the experimental period under our conditions (Fig. 4, H and I). Together, these results indicate that JIPs restore epithelial TJs in a mouse intestinal epithelial injury model and therefore reduce symptom onset.

In humans, 36- to 44–amino acid polypeptides corresponding to the C terminus of hA1AT are present in circulating blood of patients with sepsis, nipple aspiration fluid of patients with breast cancer, and urine of patients with glomerulonephritis (*12*–*14*). These peptides include JIP_{h42}/CAAP48, a biomarker of sepsis (*12*). Therefore, we assessed the TJ-inducing activity of JIP_{h42}/CAAP48. JIP_{h42}/CAAP48 induced claudin assembly at cell-cell boundaries and increased the barrier activity in A431 cell monolayers at the same concentrations as JIP_{m35} (JIP_{h42}/CAAP48; Fig. 5, A to D). Claudin-assembling activity was significantly reduced when mutations were introduced into hydrophobic clusters of JIP_{h42}/CAAP48 ($JIP_{h42\text{-}mut1}$, $JIP_{h42\text{-}mut2}$, and $JIP_{h42\text{-}mut3}$; Fig. 5, A to D), which suggested that hydrophobic amino acid clusters are essential for the TJ-assembling activity of JIP_{h42}/CAAP48 similar to mouse JIPs. This was confirmed by the in vitro G_{13} activation assay, in which G_{13} activity was increased by JIP_{h42}/CAAP48, $JIP_{h42\text{-}mut3}$, and $JIP_{h42\text{-}mut4}$, but not by $JIP_{h42\text{-}mut1}$ or $JIP_{h42\text{-}mut2}$ (Fig. 5E), which indicated that JIP_{h42}/CAAP48 directly activated G_{13} through the N-terminal hydrophobic cluster. Next, we examined whether human CAAP48 had a similar tissue repair activity. JIP_{h42}/CAAP48 administration sustained epithelial TJs (Fig. 5, F and G) and ameliorated hematogenous diarrhea (Fig. 5H) and infiltration of Gr-1–positive neutrophils into epithelial layers (Fig. 5, I and J) of DSS-treated mice. Because N-terminal hydrophobic amino acids were conserved in both JIP_{m35} and JIP_{h42}/CAAP48, these hydrophobic clusters may be essential for the DSS colitis–alleviating activity. These data indicate that the TJ-induced tissue-repairing activity of A1AT C-terminal peptides is conserved in mice and humans.

DISCUSSION

TJ formation is regulated by extracellular factors. For example, treatment of cells with trypsin or nonspecific serine proteases induces TJ formation (*36*–*38*), and a series of proteinase-activated receptors regulate TJ formation (*39*). Urine extracts from animals exhibit TJ-enhancing activity associated with epidermal growth factor (*40*, *41*). In this study, we showed that C-terminal fragments of anti-inflammatory protein A1AT were physiological JIPs that induced TJ formation in response to tissue damage. JIPs penetrated plasma membranes and induced TJ assembly by directly activating G_{13}. Since cell-penetrating peptides penetrate preferentially to inflammatory cells or cancer cells, which have high membrane permeability (*42*, *43*), JIP_{m35} may penetrate plasma membrane of damaged intestinal epithelial cells in DSS-treated mice. G_{13} stimulates Rho signaling by directly activating RhoGEFs, such as PDZ-RhoGEF and p115-RhoGEF (*44*), which leads to cortical actin remodeling. Because junctional actin is essential to regulating apical junctional complexes, whereby adhesion receptors accumulate at nascent adhesion sites (*45*), we speculate that the JIPm35-G_{13} axis induces TJ assembly by activating RhoGEF-Rho-cortical actin remodeling (Fig. 4J).

A1AT is an abundant serine protease inhibitor in serum and has important roles in suppression of inflammation and tissue destruction by inhibiting serine proteases. However, additional unclear mechanisms have been suggested (*46*). A1AT deficiency predisposes patients to the onset of various inflammatory diseases, including chronic obstructive pulmonary disease, cirrhosis, and colitis (*18*). FL-A1AT binds irreversibly to elastase, a serine protease released from neutrophils during inflammation, and inhibits its activity to avoid connective tissue degradation caused by persistent activation of elastase (*18*). In addition to FL-A1AT, C-terminal peptides of A1AT are present in patients with inflammatory diseases and cancer

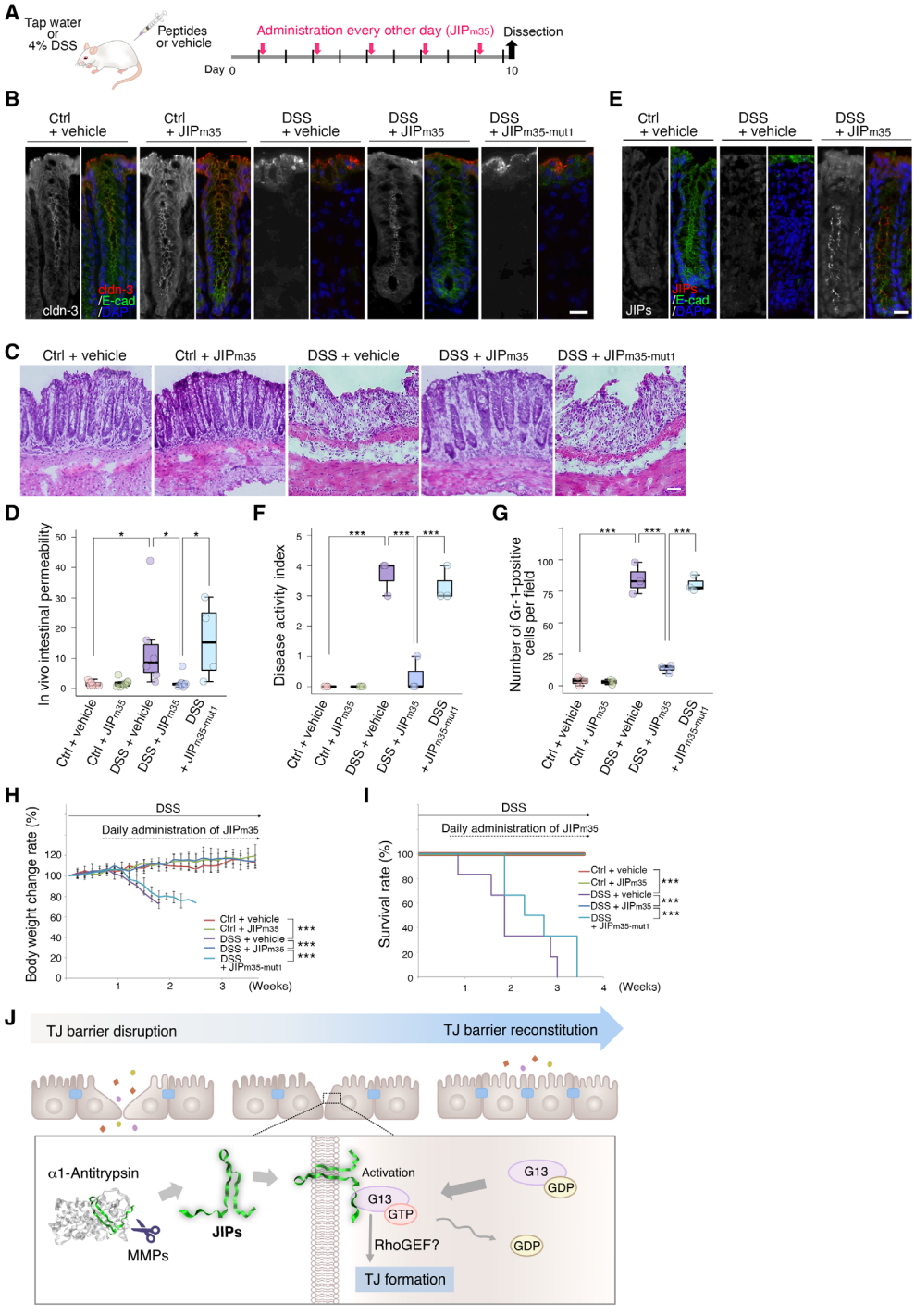

Fig. 4. Administration of JIPs restores TJs and ameliorates the symptoms of the DSS-induced colitis model in mice. (**A**) Schema of JIP_{m35} administration to DSS-induced colitis mice. (**B**) Immunofluorescence of claudin-3 and E-cadherin in colon sections from mice treated with DSS or tap water with 2.3 mg/kg per dose JIP_{m35}, $JIP_{m35\text{-}mut1}$, or the vehicle control for 10 days. Scale bar, 20 μm. Similar results were obtained in two independent experiments. (**C**) H&E staining of colon sections on day 10. Scale bar, 50 μm. Similar results were obtained in two independent experiments. (**D**) Relative intestinal permeability measured by plasma leakage of FITC-dextran (4 kDa) (ctrl + vehicle, DSS + JIP_{m35}; $n = 8$ mice, ctrl + JIP_{m35}; $n = 7$ mice, DSS + vehicle; $n = 6$ mice, DSS + $JIP_{m35\text{-}mut1}$; $n = 4$ mice). (**E**) Immunofluorescence of JIP_{m35} and E-cadherin in colon sections from mice treated with DSS or tap water with 11.1 mg/kg JIP_{m35} or the vehicle control for 10 consecutive days. Scale bar, 20 μm. Similar results were obtained in two independent experiments. (**F**) DAI in accordance with assessment of stool consistency and fecal blood ($n = 3$ mice). (**G**) Quantification of the numbers of Gr-1–positive cells in colon sections from mice treated as described in Fig. 4A ($n = 3$ images from three mice). See fig. S11D. (**H**) Body weight changes in mice treated with DSS or tap water with daily administration of JIP_{m35}, $JIP_{m35\text{-}mut1}$, or the vehicle control for up to 25 consecutive days at 1.1 mg/kg per day. Peptide administration started 4 days after DSS treatment ($n = 4$ mice). (**I**) Kaplan-Meier survival curve of mice treated as in (H) ($n = 6$ mice). (**J**) Model of TJ formation by JIPs through direct G_{13} activation during tissue repair. Tukey's test (D, F, and G), Kruskal-Wallis test (H), and log-rank test (I). $^*P < 0.05$, $^{***}P < 0.001$.

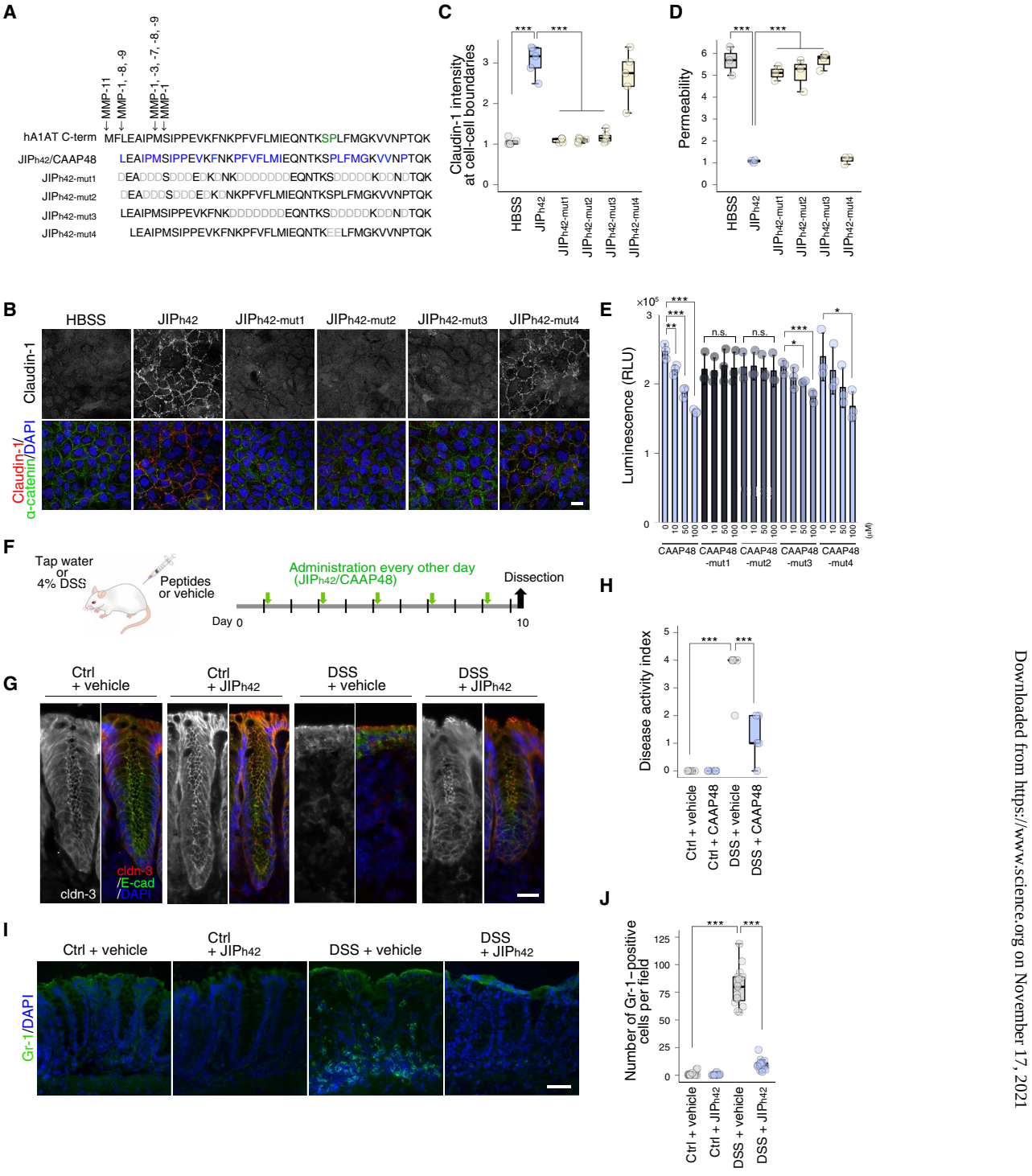

Fig. 5. Human A1AT C-terminal peptides induce TJ assembly in A431 cells and DSS-induced colitis mice. (**A**) Amino acid sequences of the human A1AT C terminus, JIP_{h42}/CAAP48, and mutant forms of JIP_{h42}/CAAP48 used in this study. (**B**) Immunofluorescence of claudin-1 and α-catenin in A431 cells treated with the indicated peptides at 20 μM or control HBSS for 3 hours. Scale bar, 20 μm. (**C**) Quantification of relative claudin-1 intensity at cell-cell boundaries of A431 cells shown in (B) ($n = 5$ images from independent two samples). Similar results were obtained in two independent experiments. (**D**) Relative barrier permeability measured by paracellular tracer flux analysis using FITC-dextran (4 kDa) in A431 cells treated as in (B) and (C) ($n = 3$ independent samples). (**E**) Measurement of G_{13} activation in the presence of JIP_{h42}, JIP $_{h42\text{-}mut1}$, JIP $_{h42\text{-}mut2}$, JIP $_{h42\text{-}mut3}$, and JIP $_{h42\text{-}mut4}$, which was assayed in GEF buffer with 5 pmol G_{13}, 10 μM GTP, and 10 mM DTT. Synthetic peptides were prepared at the indicated concentrations ($n = 3$ independent samples). (**F**) Schema of JIP_{h42}/CAAP48 administration to DSS-induced colitis mice. (**G**) Immunofluorescence of claudin-3 and E-cadherin in colon sections from mice treated with DSS or tap water with 1.5 mg/kg per dose JIP_{h42}/CAAP48 or vehicle control for 10 days. Scale bar, 20 μm (**H**) DAI in accordance with assessment of stool consistency and fecal blood ($n = 5$ mice). (**I**) Immunofluorescence of Gr-1 in colon sections from mice treated as in (F). Scale bar, 40 μm. (**J**) Quantification of the numbers of Gr-1–positive cells shown in (I) (ctrl + vehicle, ctrl+ JIP_{h42}; $n = 14$ images, DSS + vehicle, DSS + JIP_{h42}; $n = 15$ images from five mice each). Dunnett's test (C to E, H, and J). ***$P < 0.001$.

(*12*–*14*), although their physiological functions have not been clarified. Our study revealed a TJ-inducing activity of A1AT C-terminal peptides, which was independent of serine protease inhibitory activity. The amount of JIPs was increased upon tissue damage and during repair processes, which suggested that cleavage of FL-A1AT is mediated by inflammatory regulators. JIPs are generated by cleavage of FL-A1AT by MMPs, which are secreted from neutrophils and macrophages in inflammation (*47*), suggesting involvement of inflammatory-related immune cells in this process. The balance of epithelial damage and the amount of JIPs is critical for tissue recovery. Upon tissue damage, A1AT exerted anti-inflammatory effects via two mechanisms: FL protein suppressed elastase activity, and C-terminal peptides reconstituted epithelial TJs.

Sixty and 36 serine protease inhibitor (serpin) genes have been reported in mice and humans, respectively (*48*). Our MS analysis identified C-terminal peptides of serpin other than A1AT (source data fig. 9). Since C-terminal regions of some other serpins are structurally conserved (*48*), it would be interesting to determine whether C-terminal peptides released from FL-serpins also have a TJ-inducing activity. Hydrophobic clusters in the C-terminal region of A1AT are evolutionally conserved in vertebrates, which suggests that JIP-mediated TJ formation is a common anti-inflammatory response against barrier dysfunction. Thus, JIP administration might be a novel therapeutic strategy for TJ disruption in inflammatory diseases.

MATERIALS AND METHODS

Mice

Mice were housed individually in controlled environmental conditions at 22° ± 2°C, with a 12-hour light-dark cycle and ad libitum access to food and tap water. All experiments were performed in accordance with the guidelines of the Kyoto University Regulation on Animal Experimentation. All procedures for animal experiments were approved by the animal experiments committee of the Institute for Frontier Life and Medical Sciences, Kyoto University. Institute of Cancer Research (ICR) female mice (8 weeks old) were purchased from Shimizu Laboratory Supplies. *Lgr5-EGFP-IRES-creERT2/tdTomato* mice were gifts from R. Kageyama and T. Tateya. Tamoxifen (4 mg) was injected intraperitoneally twice before DSS treatment.

Colon-conditioned medium

The colon (0.1 μg) was harvested from 8- to 12-week-old ICR mice (Shimizu Laboratory Supplies) and cultured in 0.4 ml of Hanks' balanced salt solution (HBSS; 14025, Gibco) for 18 hours. The supernatant was collected and boiled for 10 min. After centrifugation, the supernatant was filtrated through a 0.22-μM Millex-GV filter (Millipore).

Peritoneum-conditioned medium

The peritoneum was harvested from 8- to 12-week-old ICR mice (Shimizu Laboratory Supplies) and cultured in 0.7 ml of HBSS (14025, Gibco) for 18 hours. The supernatant was collected and boiled for 10 min. After centrifugation, the supernatant was filtrated through a 0.22-μm Millex-GV filter (Millipore). Thirty mice yielded ~15 ml of PCM. LPS-stimulated PCM was prepared from mice injected intraperitoneally with LPS (10 mg/kg).

Purification of TJ-inducing factors

PCM (8 ml) was subjected to chromatography on Q Sepharose (GE Healthcare) and eluted with a stepwise pH gradient. The active fractions (pH 4.5 to 3.0) were further subjected to chromatography on Con A Sepharose (GE Healthcare) and eluted with 0.5 M mannoside. The eluted fraction was applied to nano-LC/MS/MS. The immunoprecipitants with anti-A1AT antibody from 24 ml of PCM were treated with 8 M urea and glycine-HCl (pH 2.6). The eluted substances were applied to a C18 column (Inertsil ODS-3, GL Sciences) on a high-performance LC system (Shimadzu). The injection volume was set to 100 μl, and the flow rate was 800 μl/min. The mobile phases consisted of (A) 0.5% acetic acid and (B) 0.5% acetic acid in 80% acetonitrile. Two-step linear gradient programs ranging from 5 to 99% B were used.

Nano–liquid chromatography tandem mass spectrometry

Nano-LC/MS/MS was conducted using a Q Exactive mass spectrometer (Thermo Fisher Scientific) or an Orbitrap Fusion Lumos mass spectrometer (Thermo Fisher Scientific) equipped with an Ultimate 3000 pump (Thermo Fisher Scientific) and an HTC-PAL autosampler (CTC Analytics). Peptides were separated by a self-pulled analytical column (150 mm length by 100 μm internal diameter) packed with ReproSil-Pur C18-AQ materials (3 μm, Dr. Maisch, Germany). The injection volume was set to 5 μl, and the flow rate was 500 nl/min. The mobile phases consisted of (A) 0.5% acetic acid and (B) 0.5% acetic acid in 80% acetonitrile. Two-step linear gradient programs ranging from 5 to 99% B over 50 to 90 min were used. An MS1 survey scan followed by MS2 scans were performed according to the data-dependent acquisition mode.

Peptide/protein identification

Peptides were identified by automated database searching using Mascot v2.6 (Matrix Sciences) against UniprotKB/Swiss-Prot (release 2017/04) with a precursor mass tolerance of 5 or 10 ppm, a fragment ion mass tolerance of 0.02 Da or 20 ppm, and strict trypsin/P specificity allowing up to two missed cleavages. Cys carbamidomethylation was set as a fixed modification, and Met oxidation was set as a variable modification. Peptides were identified if the Mascot score was over the 95% confidence limit ($P < 0.05$) for each peptide; at least two identified peptides per protein were required for protein identification except for immunoprecipitated samples. Note that the standard target-decoy approach could not be used as the identification number was too small (*49*).

Cell culture

A431 cells [Japanese Collection of Research Bioresources Cell Bank (JCRB)], EpH4 cells (a gift from E. Reichmann, University Children's Hospital Zurich, Switzerland), L cells, and HeLa cells were cultured in Dulbecco's modified Eagle's medium (DMEM) supplemented with 10% fetal calf serum (FCS). MCF7 cells (RIKEN BRC) were cultured in Eagle's Minimum Essential Medium (Wako) supplemented with 10% FCS and 1% nonessential amino acids. HT29 cells (American Type Culture Collection) were cultured in McCoy's 5A (Gibco) supplemented with 10% FCS. Cell cultures were incubated at 37°C in a humidified 5% CO_2 atmosphere. cDNA transfection was performed using the Lipofectamine LTX Reagent (Invitrogen) according to the manufacturer's instructions. The following G alpha agonists and antagonists were used: cholera toxin A subunit (036-20601, Wako), *P. multocida* (01-507, BioAcademia), pertussis toxin (168-22471, Fujifilm/Wako), NF-449 (1391/10, R&D Systems), and YM-254890 (257-000631, Fujifilm/Wako).

Peptide treatment

Synthetic peptides were manufactured by SynPeptide Co. Ltd. Each peptide was dissolved in 30% AcOH (JIP_{m40}, JIP_{m36}, JIP_{m35}, $JIP_{m35\text{-}mut3}$,

JIP_{h42}/CAAP48, and $JIP_{h42\text{-}mut3}$), MilliQ ($JIP_{m35\text{-}mut1}$, $JIP_{h42\text{-}mut1}$, and $JIP_{h42\text{-}mut2}$), or 2% NaOH ($JIP_{m35\text{-}mut2}$ and $JIP_{h42\text{-}mut3}$). The stock solution concentration was 25 μg/μl. The peptide solutions were added to the cell cultures at 20 μM in HBSS buffer after neutralization to pH 7.0, unless indicated otherwise in the legends, for 3 hours.

Small interfering RNA

The siRNA targeted sequences used were the following: mouse *GNA12* (5′-GCGACACCAUCUUCGACAATT-3′; SI02736958, Qiagen), mouse *GNA13* (5′-CCAUAAUCCUCUUCUUAAATT-3′; SI02670157, Qiagen), human *GNA12* (5′-GGAUCGGCCAGCUGAAUUATT-3′; SI00096558, Qiagen), and human *GNA13* (5′-CAAGGGUUUUCUUACAAUAtt-3′; S20992, Ambion). Transfection was performed using the Lipofectamine RNAiMax Reagent (Invitrogen) according to the manufacturer's instructions.

Antibodies

The following primary antibodies were used: claudin-1 polyclonal antibody (1:1000; 51-9000, Thermo Fisher Scientific), claudin-3 polyclonal antibody (1:1000; 34-1700, Thermo Fisher Scientific), claudin-4 monoclonal antibody (3E2C1, 1:1000; 32-9400, Thermo Fisher Scientific), claudin-4 monoclonal antibody Alexa Fluor 488 (3E2C1, 1:500; 329488, Thermo Fisher Scientific), ZO-1 polyclonal antibody (1:1000; 61-7300, Thermo Fisher Scientific), ZO-2 polyclonal antibody (1:1000; 71-1400, Thermo Fisher Scientific), α-catenin monoclonal antibody (1G5, 1:1000; MA1-2000, Thermo Fisher Scientific), α-catenin polyclonal antibody (1:2000; C2081, Sigma-Aldrich); E-cadherin antibody (ECCD-2, 1:1000; M108, Takara), CD144 (VE-cadherin) monoclonal antibody (BV13, 1:100; 16-1441-81, eBioscience), keratin 5 polyclonal antibody (1:500; PRB-160P, Covance), rabbit immunoglobulin G (IgG) isotype control (1:100; 02-6102, Thermo Fisher Scientific), A1AT polyclonal antibody (1:100; A0012, Dako), Gr-1 monoclonal antibody (RB6-8C5, 1:100; 14-5931-81, eBioscience), CD16/CD32 monoclonal antibody (2.4G2, 1:25; 70-0161-U500, TONBO), fluorescein isothiocyanate (FITC) CD11b monoclonal antibody (M1/70, 1:100; 35-0112-U100, TONBO), anaphase-promoting complex (APC) Ly-6G (Gr-1) monoclonal antibody (RB6-8C5, 1:100; 20-5931-U025, TONBO), $G\alpha_{12}$ monoclonal antibody (1:100; sc-515445, Santa Cruz Biotechnology), GNA12 polyclonal antibody (1:500; ab154004, Abcam), $G\alpha_{13}$ monoclonal antibody (6F6-B5, 1:100; sc-293424, Santa Cruz Biotechnology), GNA13 monoclonal antibody (E-12, 1:500; ab128900, Abcam), and glyceraldehyde-3-phosphate dehydrogenase (GAPDH) polyclonal antibody (1:500; 2275-PC-100, Trevigen). ZO-1 monoclonal antibody T8-754 and occludin monoclonal antibody MOC-37 were gifts from M. Furuse (National Institute for Physiological Sciences, Japan). Homemade rabbit polyclonal antibodies against JIPs (used at 1:500 for immunofluorescence and 1:50 for inhibitory antibodies assay) were raised against a keyhole limpet hemocyanin–conjugated peptide encoding amino acids 379 to 413 of mouse A1AT1B. The following secondary antibodies were used: Alexa 488–conjugated donkey anti-rat and anti-mouse IgG (1:1000; Jackson ImmunoResearch Laboratories); Cy3/Cy5–conjugated donkey anti-rat, anti-mouse, and anti-rabbit IgG (1:1000; Jackson ImmunoResearch Laboratories); horseradish peroxidase (HRP)–conjugated anti-rabbit IgG (1:1000; GE Healthcare); streptavidin-HRP conjugate (1:2000; RPN1231, GE Healthcare); and 4′,6-diamidino-2-phenylindole (DAPI; 1:2000; 34007971, Dojindo).

Immunofluorescence staining

Cultured cells were fixed with 1% formaldehyde in phosphate-buffered saline (PBS) for 10 min at room temperature, treated with 0.2% Triton X-100 in PBS for 10 min, and washed with PBS. Subsequently, samples were blocked with 1% bovine serum albumin for 10 min, incubated with primary antibodies for 30 min, washed, and then incubated with secondary antibodies for 30 min. For Gr-1 staining, Blocking One (Nacalai Tesque) was used as the blocking solution. Samples were mounted in FluorSave (Calbiochem). For frozen tissue sections, dissected samples were frozen in liquid nitrogen, and 5-μm-thick sections were prepared using a cryostat (Leica Microsystems). Before fixation, A431 cells were plated in 24-well plates (5×10^4 cells per well) and cultured for 4 days. MCF7 cells were plated in 24-well plates (8×10^4 cells per well) and cultured for 3 days. HT29 cells were plated in 24-well plates (2.4×10^5 cells per well) and cultured for 2 days. EpH4 cells were plated in 24-well plates (2×10^5 cells per well) and cultured for 3 days. L cells were plated in 24-well plates (8×10^4 cells per well) and cultured for 2 days. HeLa cells were plated in 24-well plates (6×10^4 cells per well) and cultured for 2 days. For immunofluorescence of colon sections, image acquisition was performed using a wide-field fluorescence microscope (IX81-ZDC, Olympus) using a 40× oil immersion objective lens (UPlanSApo/NA0.95). All other images were obtained using an inverted confocal fluorescence microscope (Leica Microsystems, TCS SP8 with a Hybrid Detector) with an oil immersion objective lens (40× HC PL APO/NA1.3, 100× HCX PL APO/NA1.46) and LAS-X software.

Quantification of relative TJ formation

The methodology for evaluating the formation rate of TJ at the cell-cell border comprised the following steps. First, a Gaussian filter was applied to the immunofluorescence images of α-catenin to suppress image intensity fluctuations that cause many spurious edges in the later steps. Second, the rotational-watershed algorithm (*50*) and binarization were used to obtain border candidates. A candidate was identified as a cell-cell border if the number of its component pixels was larger than the threshold. Last, the relative TJ formation at a border was obtained by the average pixel intensity of claudin at the border. For fig. S8 (F and H), the total fluorescence intensity of ZO-1 was divided by the total area of DAPI. The value relative to the one value of HBSS was calculated and presented.

Statistical analyses

The respective *n* values are shown in the figure legends. The *P* values were obtained by *t* test, Dunnett's test, Tukey's test, Kruskal-Wallis test, or log-rank test. For Figs. 3 (F and G) and 5E, means ± SD were calculated and presented in bar graphs. Other data were presented as box and whisker plots using R, where horizontal lines represent median values, boxes encompass values between the first and third quartiles, and whiskers give the 1.5-times interquartile range.

Paracellular flux

To measure the paracellular tracer flux, 1×10^4 cells per well were plated in Transwells (3413, Corning) and cultured for 4 days. After treatment with peptides or PCM on both apical and basolateral sides, 4 kDa FITC-dextran (FD4, Sigma-Aldrich) was added to the upper well at 1 mg/ml. After 1 hour, a medium aliquot was collected from the bottom well. The paracellular tracer flux was determined as the fluorescence intensity of FITC-dextran, which was measured

with a fluorometer (ARVO X3, PerkinElmer). The PBS blank fluorescence value was subtracted from the experimental value, and the relative value was calculated and presented.

TER measurement

Cells were plated on Transwell polycarbonate filters (Corning, 6.5 mm in diameter, three filters for each sample). A431 cells, MCF7 cells, HT29 cells, or EpH4 cells were plated at a density of 5×10^4, 6×10^4, 9×10^5, or 1.6×10^4 cells per well, respectively. After treatment with peptides on both apical and basolateral sides for 3 hours, TER was measured using a Millicell ERS-2 electrical resistance system (Merck Millipore). The TER values were calculated by subtracting the background TER of blank filters and by multiplying by the surface area of the filter.

Freeze-fracture electron microscopy

JIP_{m35}-treated A431 cells were fixed using 0.1 M phosphate buffer containing 4% formaldehyde for 1 hour at 4°C and cryo-protected by overnight incubation with PBS containing 30% glycerol and 0.01% sodium azide at 4°C. The cells were snap frozen by immersion in liquid nitrogen. A replica membrane was prepared using a JFD-II freeze-etching system (JEOL). The frozen cells were fractured with a metal knife cooled to −150°C and shadowed by unidirectional platinum-carbon evaporation from a 60° angle, followed by rotary carbon evaporation from the top. The cell debris was digested in a solution containing 2.5% SDS, 20% sucrose, and 15 mM tris-HCl (pH 8.3), for 20 min at 121°C. The replicas were immunostained using anti–claudin-1 antibody (Thermo Fisher Scientific), followed by anti-rabbit antibody conjugated to 15-nm colloidal gold (BBI Solutions). The replicas were imaged by a JEM-1010 electron microscope (JEOL) equipped with a 4 k × 4 k complementary metal-oxide semiconductor (CMOS) camera TemCam F416 (TVIPS).

Western blotting and silver staining

For Western blotting, A431 cells were lysed with buffer containing 1% SDS, 50 mM tris-HCl (pH 7.5), and 150 mM NaCl. Dried CCM was eluted in Laemmli buffer, and 35 μg of proteins was loaded for each lane. After boiling in Laemmli sample buffer, the samples were separated by SDS–polyacrylamide gel electrophoresis (SDS-PAGE) and transferred onto Immobilon-P polyvinylidene difluoride membranes (Millipore). The Western blotting procedure was performed as previously described (*51*). Signals were detected using Western Lightning Plus-ECL (PerkinElmer) and a LAS 4000 mini imaging system (Fujifilm). Band intensities were quantified using Imagequant software (Molecular Dynamics). For silver staining, the samples were separated by tricine–SDS-PAGE and stained with 2D-Silver Stain Reagent II (Cosmo Bio).

Liposome binding assay

Coatsomes EL-01-A (YUKA SANGYO) were suspended in H_2O at 5 mg/ml, and liposomes were formed with stirring. Biotinylated peptides or IgG (134303, BioLegend) were mixed with streptavidin-FITC (0.25 μg; 405201, BioLegend) for 30 min. Biotin-streptavidin complexes were incubated with liposomes (0.25 mg) in 100 μl of H_2O for 30 min at room temperature and were then centrifuged at 23,200*g* for 60 min at 25°C. The fluorescence intensity of supernatants and pellets was measured with a fluorometer (ARVO X3, PerkinElmer). Relative fluorescence unit values were presented.

Antibody transfection and microinjection

Anti-JIP serum or preimmune serum was transfected into A431 cells by ProteoCarry (Funakoshi) according to the manufacturer's instructions. Microinjection of anti-JIPs serum or preimmune serum was performed using a digital microinjection system (Eppendorf, FemtoJet).

Phase separation assay

ZO-1–green fluorescent protein (GFP) was purified as previously described (*27*). ZO-1–GFP was diluted from storage buffer into phase separation buffer [20 mM Hepes (pH 7.4), 150 mM NaCl, and 2% poly(ethylene glycol)] to the indicated concentration. For testing the peptide influence on ZO-1–GFP phase separation, the indicated peptide is added to the ZO-1–GFP storage first and then diluted to the phase separation buffer.

Lipid-coated beads recruitment assay

Silica beads (10 μm; C-SIO-10.0, Corpuscular) were coated with a supported lipid bilayer as described (*52*) with 1-palmitoyl-2-oleoyl-glycero-3-phosphocholine (POPC; 850457C, Avanti). The lipid bilayer was labeled with 0.1% DPPE-KK114 (1,2-dipalmitoyl-*sn*-glycero-3-phosphoethanolamine). The lipid-coated beads are incubated with the indicated peptide (5 μM) for 2 hours in buffer A [20 mM Hepes (pH 7.4) and 150 mM NaCl]. Uninserted peptides were washed away with buffer A for six times. ZO-1–GFP (100 nM) was then added to the beads for 30 min. Ten percent L-α-phosphatidylinositol-4,5-bisphosphate (porcine brain, 840046X, Avanti) (ammonium salt) [$PI(4,5)P_2$], 90% POPC-coated beads was used as a positive control.

The activity of Gα proteins assay

The activity of Gα proteins (Abcam) was measured using GTPase-Glo assay (V7681, Promega) according to the manufacturer's instructions. The assay was performed in GEF buffer containing 5 pmol Gα, 10 μM guanosine 5′-triphosphate (GTP), and 10 mM dithiothreitol (DTT). Relative light unit values were presented.

Pull-down experiments

A431 cells treated with biotinylated-JIP_{m35}, biotinylated-$JIP_{m35\text{-}mut2}$, or control HBSS buffer were lysed with radioimmunoprecipitation assay buffer (1% NP-40, 0.1% SDS, 0.5% sodium deoxycholate, 50 mM tris-HCl, and 150 mM NaCl). Pull down was performed with Streptavidin Sepharose (GE Healthcare), and the precipitates were eluted by boiling in SDS sample buffer. The samples were separated by SDS-PAGE or tricine–SDS-PAGE and immunoblotted with anti-G_{12} (upper), G_{13} (middle), and streptavidin-HRP conjugate antibodies (bottom).

Dialysis

A dialysis membrane was prepared according to the manufacturer's instructions. The PCM was dialyzed twice at 4°C with HBSS for 2 hours and then overnight. A Micro Float-A-Lyzer device with MWCO 500–1000 D (Spectra) was used for a 1-kDa cutoff, and Oscillatory Microdialysis System with MWCO 3500 cup (Bio-Tech) was used for a 3.5-kDa cutoff.

Matrix metalloproteinases

Recombinant MMP-1, MMP-8, or MMP-9 (1 μg; R&D Systems) was activated by 1 mM *p*-aminophenylmercuric acetate (A9563; Sigma-Aldrich) at 37°C for 2 hours (MMP-1 and MMP-8) or

24 hours (MMP-9). FL recombinant hA1AT (40 μM; A6150, Sigma-Aldrich) was incubated with the indicated MMP at 37°C for 24 hours. For MMP inhibition, MMP inhibitor GM6001 (50 μM; ab120845, Abcam) was added to the colon culture.

Measurement of protease activity

Protease activity was measured with an Amplite Universal Fluorimetric Protease Activity Assay Kit according to the manufacturer's instructions. For trypsin assays, the kit's components were used. Human neutrophil elastase (HNE) (0.5 μM; ab91099, Abcam) was analyzed in 100 mM tris-HCl (pH 7.5) and 500 mM NaCl. Porcine pancreas elastase (PPE) (0.5 μM; V189A, Promega) was analyzed in 10 mM tris-HCl (pH 9.0). Chymotrypsin (0.5 μM; V106A, Promega) was analyzed in 100 mM tris-HCl (pH 8.0) and 10 mM $CaCl_2$. Data are presented as relative fluorescence units.

Isolation of mouse neutrophil

Femurs and tibias were obtained from 8-week-old mice. Bone marrow–derived neutrophils were prepared as previously described (*53*). The cells were resuspended in 1.2 ml of HBSS and 800 μl of 100% Percoll, layered over a 62.5% Percoll gradient, and centrifuged at 800*g* for 30 min. Neutrophils were harvested from the bottom layer of the gradient.

Enzyme-linked immunosorbent assays

Bone marrow–derived mouse neutrophils (2×10^6 cells/ml) from two mice were preincubated for 1 hour with or without JIP_{m35} and then treated with LPS (10 ng/ml) for 18 hours at 37°C. Culture supernatants were collected and analyzed for TNFα and CXCL1 using the kits (MTA00B and DY453, R&D Systems).

Experimental design, induction of colitis, and tissue collection

Acute colitis was induced with 4% (w/v) DSS (molecular weight, 5000 Da; Wako) dissolved in drinking water until the end of the experiment. The first day of DSS treatment was designated day 0, and all mice were sacrificed on day 10. After euthanasia, stools from mice were collected and photographed using a digital camera (NEX-5N, Sony). For histological staining, colon tissues close to the anus were collected and immediately frozen in liquid nitrogen. Hematoxylin and eosin (H&E) staining was performed with a standard protocol, and the images were obtained using an all-in-one microscope (BZ8000, Keyence) with a 20× dry objective lens (Plan Apo/NA0.75, Nikon).

For recovery period experiment, the mice were randomly assigned to two groups: group 1, control; group 2, 4% DSS-induced colitis and changed to 1% (*Lgr5-EGFP-IRES-creERT2/ROSA26td-Tomato* mice) or 2% (ICR mice) DSS on day 10. Colon (0.1 μg) was collected on days 11 and 12 ($n = 4$ for each group) and cultured for CCM. Anti-JIPs antibodies or preimmune serum was injected on days 9 and 11 ($n = 6$ for each group; 250 μl injection per mice).

For JIP_{m35} administration analysis, the mice were randomly assigned to five groups: group 1, control treated with vehicle ($n = 5$); group 2, control treated with JIP_{m35} ($n = 5$); group 3, DSS-induced colitis treated with vehicle ($n = 5$); group 4, DSS-induced colitis treated with JIP_{m35} ($n = 5$); and group 5, DSS-induced colitis treated with $JIP_{m35\text{-}mut1}$ ($n = 5$). Mice receiving drinking tap water alone were used as controls. JIP_{m35} or $JIP_{m35\text{-}mut1}$ peptides (2.3 mg/kg per dose) were subcutaneously administered to mice every other day.

For JIP_{h42}/CAAP48 administration analysis, mice were randomly assigned to four groups: group 1, control treated with vehicle ($n = 5$); group 2, control treated with JIP_{h42}/CAAP48 ($n = 5$); group 3, DSS-induced colitis treated with vehicle ($n = 5$); and group 4, DSS-induced colitis treated with JIP_{h42}/CAAP48 ($n = 5$). Mice receiving drinking tap water alone were used as controls. JIP_{h42}/CAAP48 peptides (1.5 mg/kg per dose) were subcutaneously administered to mice every other day.

Intestinal permeability assay

Mice ($n = 8$ for each group) were fasted for 4 hours, and 4-kDa FITC-dextran (80 mg/ml in PBS, 150 μl per mouse; FD-4, Sigma-Aldrich) was applied orally at a single dose. Blood was collected 4 hours after gavage, and plasma was obtained after centrifugation at 2000*g* for 5 min. Plasma samples were diluted 1:10 in PBS and transferred to a black opaque-bottom 96-well plate. Fluorescence was determined as the fluorescence intensity of FITC-dextran measured with a fluorometer (ARVO X3, PerkinElmer). The PBS blank fluorescence value was subtracted from the experimental value, and the value relative to the one value of control was calculated and presented.

Disease activity index

The disease activity index (DAI) for DSS colitis was scored according to the mean of two parameters: stool consistency and fecal blood. The scoring system was as follows: stool consistency—0 = well-formed pellets, 1 = soft, and 2 = diarrhea; fecal blood—0 = no blood, 1 = blood traces visible outside of the stool, and 2 = blood traces visible inside and outside of the stool, gross rectal bleeding. Stool consistency scores and bleeding scores were added and presented as a clinical score. The sum of the two values constitutes the DAI, resulting in a total clinical score ranging from a minimum of 0 to a maximum of 4 ($n = 3$).

Body weight loss and survival rate

Mice ($n = 6$ for each group) were treated with 4% (w/v) DSS dissolved in drinking water until the end of the experiment, whereas the control groups received only tap water. Peptide-treated groups were subcutaneously administered JIP_{m35} or $JIP_{m35\text{-}mut1}$ (1.1 mg/kg per day) every day following the 4-day DSS treatment. The vehicle-treated animals were administered HBSS. The body weight of each mouse was monitored daily, and the percentage of body weight loss was calculated. The survival rate was analyzed by the Kaplan-Meier test.

SUPPLEMENTARY MATERIALS

Supplementary material for this article is available at https://science.org/doi/10.1126/sciadv.abj6895

View/request a protocol for this paper from *Bio-protocol*.

REFERENCES AND NOTES

1. J. M. Anderson, C. M. Van Itallie, Physiology and function of the tight junction. *Cold Spring Harb. Perspect. Biol.* **1**, a002584 (2009).
2. C. Barmeyer, J. D. Schulzke, M. Fromm, Claudin-related intestinal diseases. *Semin. Cell Dev. Biol.* **42**, 30–38 (2015).
3. A. C. Luissint, C. A. Parkos, A. Nusrat, Inflammation and the intestinal barrier: Leukocyte-epithelial cell interactions, cell junction remodeling, and mucosal repair. *Gastroenterology* **151**, 616–632 (2016).
4. S. Tsukita, M. Furuse, M. Itoh, Multifunctional strands in tight junctions. *Nat. Rev. Mol. Cell Biol.* **2**, 285–293 (2001).

5. J. R. Turner, Intestinal mucosal barrier function in health and disease. *Nat. Rev. Immunol.* **9**, 799–809 (2009).
6. S. Citi, The mechanobiology of tight junctions. *Biophys. Rev.* **11**, 783–793 (2019).
7. C. Zihni, C. Mills, K. Matter, M. S. Balda, Tight junctions: From simple barriers to multifunctional molecular gates. *Nat. Rev. Mol. Cell Biol.* **17**, 564–580 (2016).
8. A. Buckley, J. R. Turner, Cell biology of tight junction barrier regulation and mucosal disease. *Cold Spring Harb. Perspect. Biol.* **10**, (2018).
9. S. Tsukita, H. Tanaka, A. Tamura, The Claudins: From tight junctions to biological systems. *Trends Biochem. Sci.* **44**, 141–152 (2019).
10. J. C. Brazil, M. Quiros, A. Nusrat, C. A. Parkos, Innate immune cell-epithelial crosstalk during wound repair. *J. Clin. Invest.* **129**, 2983–2993 (2019).
11. D. Castillo-Azofeifa, E. N. Fazio, R. Nattiv, H. J. Good, T. Wald, M. A. Pest, F. J. Sauvage, O. D. Klein, S. Asfaha, Atoh1^{+} secretory progenitors possess renewal capacity independent of Lgr5^{+} cells during colonic regeneration. *EMBO J.* **38**, e99984 (2019).
12. M. Kiehntopf, D. Schmerler, F. M. Brunkhorst, R. Winkler, K. Ludewig, D. Osterloh, F. Bloos, K. Reinhart, T. Deufel, Mass spectometry-based protein patterns in the diagnosis of sepsis/systemic inflammatory response syndrome. *Shock* **36**, 560–569 (2011).
13. R. Machii, M. Sakatume, R. Kubota, S. Kobayashi, F. Gejyo, K. Shiba, Examination of the molecular diversity of alpha1 antitrypsin in urine: Deficit of an α1 globulin fraction on cellulose acetate membrane electrophoresis. *J. Clin. Lab. Anal.* **19**, 16–21 (2005).
14. J. Zhou, B. Trock, T. N. Tsangaris, N. B. Friedman, D. Shapiro, M. Brotzman, Y. Chan-Li, D. W. Chan, J. Li, A unique proteolytic fragment of alpha1-antitrypsin is elevated in ductal fluid of breast cancer patient. *Breast Cancer Res. Treat.* **123**, 73–86 (2010).
15. F. Yan, L. Wang, Y. Shi, H. Cao, L. Liu, M. K. Washington, R. Chaturvedi, D. A. Israel, H. Cao, B. Wang, R. M. Peek Jr., K. T. Wilson, D. B. Polk, Berberine promotes recovery of colitis and inhibits inflammatory responses in colonic macrophages and epithelial cells in DSS-treated mice. *Am. J. Physiol. Gastrointest. Liver Physiol.* **302**, G504–G514 (2012).
16. C. M. Vanitallie, M. S. Balda, J. M. Anderson, Epidermal growth-factor induces tyrosine phosphorylation and reorganization of the tight junction protein Zo-1 in A431 cells. *J. Cell Sci.* **108**, 1735–1742 (1995).
17. K. Umeda, J. Ikenouchi, S. Katahira-Tayama, K. Furuse, H. Sasaki, M. Nakayama, T. Matsui, S. Tsukita, M. Furuse, S. Tsukita, ZO-1 and ZO-2 independently determine where claudins are polymerized in tight-junction strand formation. *Cell* **126**, 741–754 (2006).
18. C. M. Greene, S. J. Marciniak, J. Teckman, I. Ferrarotti, M. L. Brantly, D. A. Lomas, J. K. Stoller, N. G. McElvaney, α1-Antitrypsin deficiency. *Nat. Rev. Dis. Primers.* **2**, 16051 (2016).
19. N. Barker, J. H. van Es, J. Kuipers, P. Kujala, M. van den Born, M. Cozijnsen, A. Haegebarth, J. Korving, H. Begthel, P. J. Peters, H. Clevers, Identification of stem cells in small intestine and colon by marker gene Lgr5. *Nature* **449**, 1003–1007 (2007).
20. P. E. Desrochers, J. J. Jeffrey, S. J. Weiss, Interstitial collagenase (matrix metalloproteinase-1) expresses serpinase activity. *J. Clin. Invest.* **87**, 2258–2265 (1991).
21. P. E. Desrochers, K. Mookhtiar, H. E. Van Wart, K. A. Hasty, S. J. Weiss, Proteolytic inactivation of alpha 1-proteinase inhibitor and alpha 1-antichymotrypsin by oxidatively activated human neutrophil metalloproteinases. *J. Biol. Chem.* **267**, 5005–5012 (1992).
22. D. Pei, G. Majmudar, S. J. Weiss, Hydrolytic inactivation of a breast carcinoma cell-derived serpin by human stromelysin-3. *J. Biol. Chem.* **269**, 25849–25855 (1994).
23. M. C. Vissers, P. M. George, I. C. Bathurst, S. O. Brennan, C. C. Winterbourn, Cleavage and inactivation of alpha 1-antitrypsin by metalloproteinases released from neutrophils. *J. Clin. Invest.* **82**, 706–711 (1988).
24. Z. Zhang, P. G. Winyard, K. Chidwick, G. Murphy, M. Wardell, R. W. Carrell, D. R. Blake, Proteolysis of human native and oxidised α 1-proteinase inhibitor by matrilysin and stromelysin. *Biochim. Biophys. Acta* **1199**, 224–228 (1994).
25. B. L. Daugherty, C. Ward, T. Smith, J. D. Ritzenthaler, M. Koval, Regulation of heterotypic claudin compatibility. *J. Biol. Chem.* **282**, 30005–30013 (2007).
26. M. Furuse, H. Sasaki, K. Fujimoto, S. Tsukita, A single gene product, claudin-1 or −2, reconstitutes tight junction strands and recruits occludin in fibroblasts. *J. Cell Biol.* **143**, 391–401 (1998).
27. O. Beutel, R. Maraspini, K. Pombo-Garcia, C. Martin-Lemaitre, A. Honigmann, Phase separation of zonula occludens proteins drives formation of tight junctions. *Cell* **179**, 923–936.e11 (2019).
28. Y. Iizuka, T. Okuno, K. Saeki, H. Uozaki, S. Okada, T. Misaka, T. Sato, H. Toh, M. Fukayama, N. Takeda, Y. Kita, T. Shimizu, M. Nakamura, T. Yokomizo, Protective role of the leukotriene B4 receptor BLT2 in murine inflammatory colitis. *FASEB J.* **24**, 4678–4690 (2010).
29. Y. Ishii, K. Saeki, M. Liu, F. Sasaki, T. Koga, K. Kitajima, C. Meno, T. Okuno, T. Yokomizo, Leukotriene B4 receptor type 2 (BLT2) enhances skin barrier function by regulating tight junction proteins. *FASEB J.* **30**, 933–947 (2016).
30. J. H. C. Orth, I. Fester, I. Preuss, L. Agnoletto, B. A. Wilson, K. Aktories, Activation of Gαi and subsequent uncoupling of Receptor-Gαi signaling by Pasteurella multocida toxin. *J. Biol. Chem.* **283**, 23288–23294 (2008).
31. J. H. Orth, S. Lang, M. Taniguchi, K. Aktories, Pasteurella multocida toxin-induced activation of RhoA is mediated via two families of Gα proteins, Gαq and Gα12/13. *J. Biol. Chem.* **280**, 36701–36707 (2005).
32. D. Cassel, T. Pfeuffer, Mechanism of cholera toxin action: Covalent modification of the guanyl nucleotide-binding protein of the adenylate cyclase system. *Proc. Natl. Acad. Sci. U.S.A.* **75**, 2669–2673 (1978).
33. M. Hohenegger, M. Waldhoer, W. Beindl, B. Boing, A. Kreimeyer, P. Nickel, C. Nanoff, M. Freissmuth, Gsα-selective G protein antagonists. *Proc. Natl. Acad. Sci. U.S.A.* **95**, 346–351 (1998).
34. T. Katada, M. Ui, Direct modification of the membrane adenylate-cyclase system by islet-activating protein due to adp-ribosylation of a membrane-protein. *Proc. Natl. Acad. Sci. U. S. A.* **79**, 3129–3133 (1982).
35. J. Takasaki, T. Saito, M. Taniguchi, T. Kawasaki, Y. Moritani, K. Hayashi, M. Kobori, A novel Gαq/11-selective inhibitor. *J. Biol. Chem.* **279**, 47438–47445 (2004).
36. E. Cohen, A. Talmon, O. Faff, A. Bacher, Y. Ben-Shaul, Formation of tight junctions in epithelial cells. I. Induction by proteases in a human colon carcinoma cell line. *Exp. Cell Res.* **156**, 103–116 (1985).
37. L. Orci, M. Amherdt, J. C. Henquin, A. E. Lambert, R. H. Unger, A. E. Renold, Pronase effect on pancreatic beta cell secretion and morphology. *Science* **180**, 647–649 (1973).
38. S. Polak-Charcon, J. Shoham, Y. Ben-Shaul, Junction formation in trypsinized cells of human adenocarcinoma cell line. *Exp. Cell Res.* **116**, 1–13 (1978).
39. R. Szabo, T. H. Bugge, Membrane-anchored serine proteases in vertebrate cell and developmental biology. *Annu. Rev. Cell Dev. Biol.* **27**, 213–235 (2011).
40. D. Flores-Benítez, A. Ruiz-Cabrera, C. Flores-Maldonado, L. Shoshani, M. Cereijido, R. G. Contreras, Control of tight junctional sealing: Role of epidermal growth factor. *Am. J. Physiol. Ren. Physiol.* **292**, F828–F836 (2007).
41. J. M. Gallardo, J. M. Hernández, R. G. Contreras, C. Flores-Maldonado, L. González-Mariscal, M. Cereijido, Tight junctions are sensitive to peptides eliminated in the urine. *J. Membr. Biol.* **188**, 33–42 (2002).
42. B. P. A. Lucke, Osmotic properties and permeability of cancer cells. I. Relative permeability of Ehrlich mouse ascites tumor cells and of mouse erythrocytes to polyhydric alcohols and to sodium chloride. *Cancer Res.* **14**, 75–80 (1954).
43. J. Xu, A. R. Khan, M. Fu, R. Wang, J. Ji, G. Zhai, Cell-penetrating peptide: A means of breaking through the physiological barriers of different tissues and organs. *J. Control. Release* **309**, 106–124 (2019).
44. P. Kelly, P. J. Casey, T. E. Meigs, Biologic functions of the G12 subfamily of heterotrimeric g proteins: Growth, migration, and metastasis. *Biochemistry* **46**, 6677–6687 (2007).
45. S. Citi, D. Guerrera, D. Spadaro, J. Shah, Epithelial junctions and Rho family GTPases: The zonular signalosome. *Small GTPases* **5**, 1–15 (2014).
46. G. Fleixo-Lima, H. Ventura, M. Medini, L. Bar, P. Strauss, E. C. Lewis, Mechanistic evidence in support of alpha1-antitrypsin as a therapeutic approach for type 1 diabetes. *J. Diabetes Sci. Technol.* **8**, 1193–1203 (2014).
47. L. Nissinen, V. M. Kahari, Matrix metalloproteinases in inflammation. *Biochim. Biophys. Acta* **1840**, 2571–2580 (2014).
48. C. Heit, B. C. Jackson, M. McAndrews, M. W. Wright, D. C. Thompson, G. A. Silverman, D. W. Nebert, V. Vasiliou, Update of the human and mouse SERPIN gene superfamily. *Hum. Genomics* **7**, 22 (2013).
49. J. E. Elias, S. P. Gygi, Target-decoy search strategy for increased confidence in large-scale protein identifications by mass spectrometry. *Nat. Methods* **4**, 207–214 (2007).
50. K. Chiba, Y. Shimada, M. Kinjo, T. Suzuki, S. Uchida, Simple and direct assembly of kymographs from movies using KYMOMAKER. *Traffic* **15**, 1–11 (2014).
51. Y. Oda, T. Otani, J. Ikenouchi, M. Furuse, Tricellulin regulates junctional tension of epithelial cells at tricellular contacts through Cdc42. *J. Cell Sci.* **127**, 4201–4212 (2014).
52. A. Cezanne, J. Lauer, A. Solomatina, I. F. Sbalzarini, M. Zerial, A non-linear system patterns Rab5 GTPase on the membrane. *eLife* **9**, (2020).
53. D. Jonigk, M. al-Omari, L. Maegel, M. Muller, N. Izykowski, J. Hong, K. Hong, S. H. Kim, M. Dorsch, R. Mahadeva, F. Laenger, H. Kreipe, A. Braun, G. Shahaf, E. C. Lewis, T. Welte, C. A. Dinarello, S. Janciauskiene, Anti-inflammatory and immunomodulatory properties of α1-antitrypsin without inhibition of elastase. *Proc. Natl. Acad. Sci. U.S.A.* **110**, 15007–15012 (2013).
54. S. Okuda, Y. Watanabe, Y. Moriya, S. Kawano, T. Yamamoto, M. Matsumoto, T. Takami, D. Kobayashi, N. Araki, A. C. Yoshizawa, T. Tabata, N. Sugiyama, S. Goto, Y. Ishihama, jPOSTrepo: An international standard data repository for proteomes. *Nucleic Acids Res.* **45**, D1107–D1111 (2017).

Acknowledgments: We thank E. Reichmann, M. Itoh, M. Furuse, and H. Katoh for providing EpH4 cells, anti–ZO-1 antibodies, and $G\alpha_{13}$ plasmids, respectively. We thank K. Tsujita for advice on liposome handling. We thank A. Yoshimura, T. Yokomizo, and T. Igaki for comments on the manuscript. We thank Y. Yanagihashi for the illustration drawing of the JIP model. We thank M. Bell, J. L. Croxford, and M. Arico from Edanz (https://jp.edanz.com/ac) for editing a draft of this manuscript. **Funding:** This work was supported by JSPS Grants-in-Aid for Scientific Research 18H02437 and 21H05286 to Y.O. and JP16H06280 to F.T., AMED-PRIME JP19gm6210014 to Y.O., the Tomizawa Jun-ichi & Keiko Fund of the Molecular Biology Society of Japan for Young Scientists to Y.O., the Takeda Science Foundation to Y.O., the Astellas Foundation for Research on Metabolic Disorders to Y.O., the Ohsumi Frontier Science Foundation to Y.O., and Joint Usage/Research Center program of the Institute for Frontier Life and Medical Sciences, Kyoto University, and Naito Grant for female scientist after maternity leave to Y.O. **Author contributions:** Y.O. and F.T. designed the experiments. Y.O., K.K., and Y. U. performed most of the experiments and analyzed the data. C.T. and Y.I. performed MS analysis. S.H. and S.U. developed a TJ quantification program and analyzed the data. S.N. and Y.F. performed the freeze-fracture experiments. H.M. performed antibody microinjection. D.S. and A.H. performed phase separation assay and lipid-coated beads experiments. Y.O. and F.T. wrote the manuscript with input from C.T., S.H., S.N., D.S., H.M., Y.F., A.H., S.U., and Y.I. **Competing interests:** Y.O., F.T., and Y.I. are inventors on a patent application related to this manuscript, which was filed by Kyoto University (2019-115248, PCT/JP2020/024154). The authors declare that they have no other competing interests. **Data and materials availability:** MS raw data and analysis files have been deposited in the ProteomeXchange Consortium (http://proteomecentral.proteomexchange.org) via the jPOST partner repository (https://jpostdb.org) (*54*) with the dataset identifier PXD01442435 (https://repository.jpostdb.org/entry/JPST000621). Code for the methodology to quantify TJ formation and draw box and whisker plots were deposited in Github (https://github.com/uchidalab/tight-junction-analysis) and Zenodo (10.5281/zenodo.5525680), respectively. All data needed to evaluate the conclusions in the paper are present in the paper and/or the Supplementary Materials.

Submitted 26 May 2021
Accepted 28 September 2021
Published 17 November 2021
10.1126/sciadv.abj6895

ScienceAdvances

Discovery of anti-inflammatory physiological peptides that promote tissue repair by reinforcing epithelial barrier formation

Yukako OdaChisato TakahashiShota HaradaShun NakamuraDaxiao SunKazumi KisoYuko UrataHitoshi MiyachiYoshinori FujiyoshiAlf HonigmannSeiichi UchidaYasushi IshihamaFumiko Toyoshima

Sci. Adv., 7 (47), eabj6895. • DOI: 10.1126/sciadv.abj6895

Science Advances (ISSN) is published by the American Association for the Advancement of Science. 1200 New York Avenue NW, Washington, DC 20005. The title *Science Advances* is a registered trademark of AAAS.